JOURNAL OF MATERIALS SCIENCE 27 (1992) 2811–2822

Interface characterization and fracture of calcium aluminosilicate glass-ceramic reinforced with Nicalon fibres

S. M. BLEAY, V. D. SCOTT, B. HARRIS, R. G. COOKE, F. A. HABIB
School of Materials Science, University of Bath, Calverton Down, Bath BA2 7AY, UK

An investigation of the structure and properties of a calcium aluminosilicate glass-ceramic reinforced with Nicalon fibres is described. Microstructural analysis of the interface showed that during manufacture of the composite a reaction zone rich in carbon formed between the Nicalon fibre and the anorthite matrix. Tensile strengths were approximately 330 MPa for unidirectional material and around 210 MPa for a $(0°/90°)_{3s}$ composite, little more than half that predicted by the mixtures rule. Flexural strengths were, however, higher than tensile strengths, by a factor 1.5–2.5 depending on lay-up. Studies carried out on specimens heat treated in air for 24 h at temperatures in the range 600–1200 °C showed a progressive change of interface microstructure in the outermost regions of the specimens due to oxidation of the carbon-rich layer; at 1000 °C and above the carbon had disappeared to leave voids and silica-rich bridges between fibre and matrix. These changes affected the strength of the interfacial bond, as measured by an micro-indentation technique, and also the degree of fibre pull-out produced in mechanical tests. Thus as-received material exhibited appreciable pull-out whilst heat-treated samples were characterized by brittle behaviour in the outer (oxidized) regions. Nevertheless, the composites whilst in the unstressed condition appeared to survive these short-term exposures to oxidizing environments. An interfacial shear stress of around 5 MPa was calculated by applying the Aveston, Cooper and Kelly theory to crack spacings measured in our room-temperature deformation experiments, a value which agreed well with the 3–5 MPa obtained by the micro-indentation method.

1. Introduction

Since the early 1970s, there has been growing interest in the reinforcement of glass and glass-ceramic systems by means of high-modulus ceramic fibres. Such a composite material offers, potentially, a combination of high specific strength and stiffness, good corrosion resistance and property retention to high temperature, and a more controlled failure mode instead of the brittle fracture characteristic of monolithic ceramics. Early work focused on carbon fibre-reinforced Pyrex [1, 2], but it was evident that the degradation of carbon fibres in oxidizing environments was a limiting factor in utilization of these materials. With the development of Nicalon [3], a silicon-carbide-based fibre, research included the Nicalon/Pyrex system [4, 5] and although offering some success, the full potential of the fibre was not utilized because the Pyrex matrix began to soften and flow well below the onset of fibre degradation. To create composites of higher application temperature, glass-ceramic matrices were therefore developed, lithium aluminosilicate (LAS) being the most widely reported [6, 7].

This paper discusses the microstructural and mechanical evaluation of calcium aluminosilicate (CAS) glass-ceramic reinforced with Nicalon fibres, a system previously studied by Cooper and Chyung [8]. The work includes detailed microstructural analyses of fibre, matrix and fibre/matrix interface, and relates the data to mechanical behaviour. Reference is made also to changes in the composite produced by heat treatment in air up to temperatures of 1100 °C.

2. Experimental procedure

2.1. Materials

Studies have been made of three plates of calcium aluminosilicate (CAS) glass-ceramic reinforced with Nicalon fibres. All were fabricated by Corning using the hot-pressing route.

The first plate, a $(0°/90°)_{3s}$ cross-ply, designated CX1, was used to characterize the as-received composite microstructure. The others, a $(0°/90°)_{3s}$ cross-ply (CX2) and a unidirectional plate (CU1), were used to study the effect on microstructure and properties of heat treatment in air. Heat treatment was carried out on samples 50 mm × 10 mm × 2 mm and heated for 24 h in air at temperatures within the range 600–1200 °C. Samples of heat-treated CU1 were subsequently tested in three-point flexure.

0022–2461 © *1992 Chapman & Hall*

2.2. Microstructural examination

A section of plate CX1 was ground into powder with a pestle and mortar and studied by X-ray diffraction (XRD) in a Philips PW1820 diffractometer. Sections were cut from each plate with a resin-bonded diamond saw at low speed and prepared for polishing by first mounting in cold curing epoxy resin. A planar specimen surface was produced by means of a diamond grinding wheel lubricated by water, followed by three polishing stages on Buehler Metlap wheels of decreasing hardness sprayed with diamond slurries of correspondingly smaller particle size in the range 9 μm down to 1 μm.

The samples were examined in a Zeiss ICM 405 optical microscope fitted with Nomarski interference contrast and, after subsequent sputter coating with carbon, by scanning electron microscopy (SEM) in a Jeol 35C equipped with backscattered electron imaging (BEI). Compositional analysis of the microstructure was carried out with a Link AN10000 energy dispersive X-ray spectrometer (EDS) fitted to the scanning electron microscope. SEM examinations were also made on the surfaces of heat-treated composite and on fractured composite plates.

To produce thin foils for examination in the transmission electron microscope (TEM), 3 mm diameter discs were first cut from bulk material with a diamond tipped coring drill. The disc was ground to a thickness of ~ 300 μm on 400 grit SiC paper, and then "dimpled" in a VCR model D500 to achieve a central specimen thickness of ~ 20 μm. Final thinning was accomplished by argon-ion bombardment in a Gatan Duomill operating at 5 kV, at an incidence angle of 15° until sample perforation and 8° to extend the thinned area. The foils were examined in a Jeol 2000FX instrument equipped with a Link AN10000 EDS system and high-angle thin-window X-ray detector. The TEM was operated in bright-field, selected-area diffraction and EDS modes.

2.3. Interface friction measurements

Interface friction measurements were carried out on polished sections of heat-treated CU1 material by means of the fibre micro-indentation technique of Marshall and Evans [9]. The technique involves loading the centre of a fibre to such an extent that it slides within the matrix. By choosing the load such that the fibre slides sufficiently to cause the indentor to contact the matrix, the interfacial friction stress, τ_i, can be calculated from

$$\tau_i = F^2/4\pi^2 u R^3 E_f \quad (1)$$

where R is fibre radius, E_f is fibre modulus (~ 200 GPa for Nicalon) and F is the force applied to the fibre calculated from

$$F = 2a^2 H \quad (2)$$

where H is the fibre hardness obtained by indenting fibres at lower loads where sliding does not occur, and a is the diagonal dimension of the indent in the fibre. The term u is the fibre depression at maximum load, and can be obtained from geometrical calculations of indent dimensions in fibre and matrix. A LECO M-400 hardness tester was used with a load of 0.5 N applied to the fibres. Tests were carried out on fibres in the interior of the composite, and at the edges where the effects of oxidation would be most severe. A value of 8.9 GPa was determined for the hardness of Nicalon fibre and used in all subsequent calculations.

2.4. Mechanical testing

Tensile strength properties were measured on parallel-sided test coupons of dimensions 20 mm × 150 mm, cut from the hot-pressed plates with a water-cooled diamond saw. Soft aluminium tabs were bonded with Araldite epoxy resin to the ends of all tensile specimens. Tensile tests were carried out in an Instron 1195 machine at a crosshead speed of 0.5 mm min^{-1}, strain measurements being made with electrical resistance strain gauges. Flexural tests were also carried out in the Instron using a three-point bending configuration with 10 mm wide samples at a span-to-depth ratio of 40 for unidirectional composites and 25 for other lay-ups. Interlaminar shear strengths (ILSS) of the unidirectional composites were measured in short-beam shear tests on samples with a span-to-depth ratio of 10.

3. Results

3.1. As-received material (CX1)

The XRD trace obtained from the ground powder, Fig. 1, was indexed as the anorthite phase, a triclinic structure with unit cell dimensions $a = 0.817\,68$ nm, $b = 1.287\,68$ nm and $c = 1.4169$ nm and a formula given as $CaAl_2Si_2O_8$ [10].

Optical microscopy, Fig. 2a, showed the composite plate to have a uniform distribution of fibres of diameter ~ 15 μm with a fibre volume fraction estimated as 0.34 ± 0.05. At higher magnification, Fig. 2b, plate-like particles of ~ 2 μm in size were visible in the matrix.

The plate-like particles were readily revealed in the SEM by means of the BEI imaging facility, Fig. 3a, their darker appearance indicating a mean atomic number lower than the surrounding matrix. The plate-like particle (P) contained primarily oxygen and aluminium, with traces of silicon and calcium, Fig. 3b.

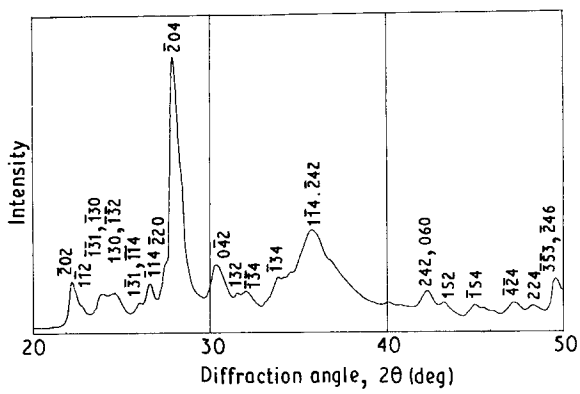

Figure 1 XRD of ground Nicalon/CAS composites with anorthite diffraction indexed.

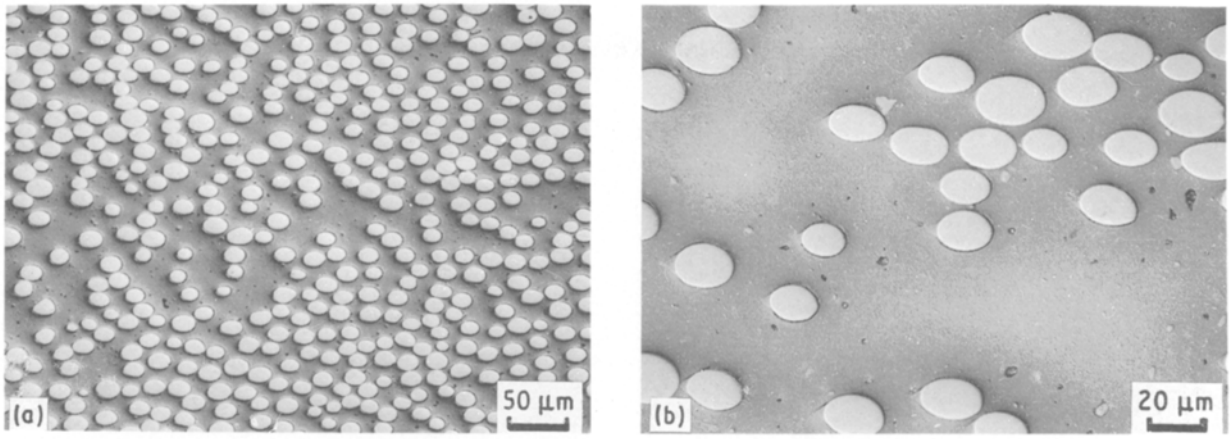

Figure 2 (a) Optical micrograph of polished unidirectional Nicalon/CAS cut at 45° to the fibre axis. (b) As (a), but at higher magnification.

EDS of the matrix region, Fig. 3c, showed it to consist of oxygen, aluminium, silicon and calcium, as expected from the specification of the CAS material; a small zirconium peak is also visible.

A transmission electron micrograph of a matrix region of CX1 is illustrated in Fig. 4a. EDS data from the matrix (Region I) and the second-phase particle (Region II) are illustrated in Fig. 4b and c, respectively, and show the matrix to consist of oxygen, aluminium, silicon and calcium as expected, and the second-phase particle to contain oxygen and aluminium. A selected-area diffraction pattern from the matrix, Fig. 4d, gives a spot pattern which can be indexed as anorthite. The spot pattern from the particle, Fig. 4e, confirmed it to be a crystal of α-Al_2O_3.

Fig. 5a reveals a number of small (~ 50 nm diameter) particles distributed at the grain boundary of an anorthite grain. EDS from a region containing one of the particles, Fig. 5b, shows a substantial amount of zirconium in addition to the peaks corresponding to the matrix composition (Fig. 4b). A finer dispersion (~ 10 nm in size) of particles of similar composition was visible within the grains.

The matrix region imaged in Fig. 6a appeared to show incomplete crystallization of the matrix. The featureless region in the centre of the micrograph is seen to be amorphous, Fig. 6b, whilst EDS data, Fig. 6c, showed it to be richer in silicon than the surrounding crystalline matrix and depleted in aluminium and calcium. No zirconium was detected in this region.

Fig. 7a shows an interface, I, between the CAS matrix and a Nicalon fibre. A particle, P, is present at the interface, the interface itself appearing as a light band ~ 150 nm thick. EDS data from the matrix, was

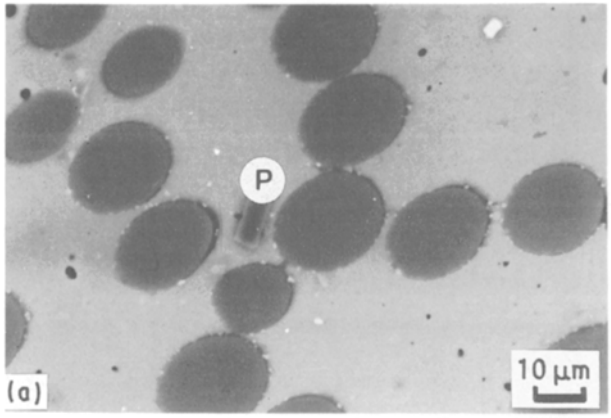

Figure 3 (a) BEI of polished Nicalon/CAS, showing a second-phase particle. (b) EDS of the CAS matrix. (c) EDS of a second-phase particle.

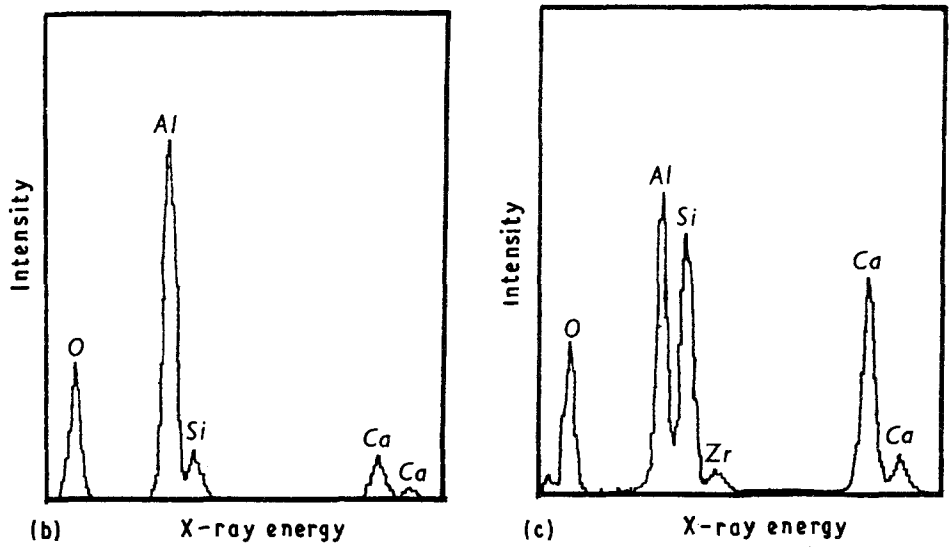

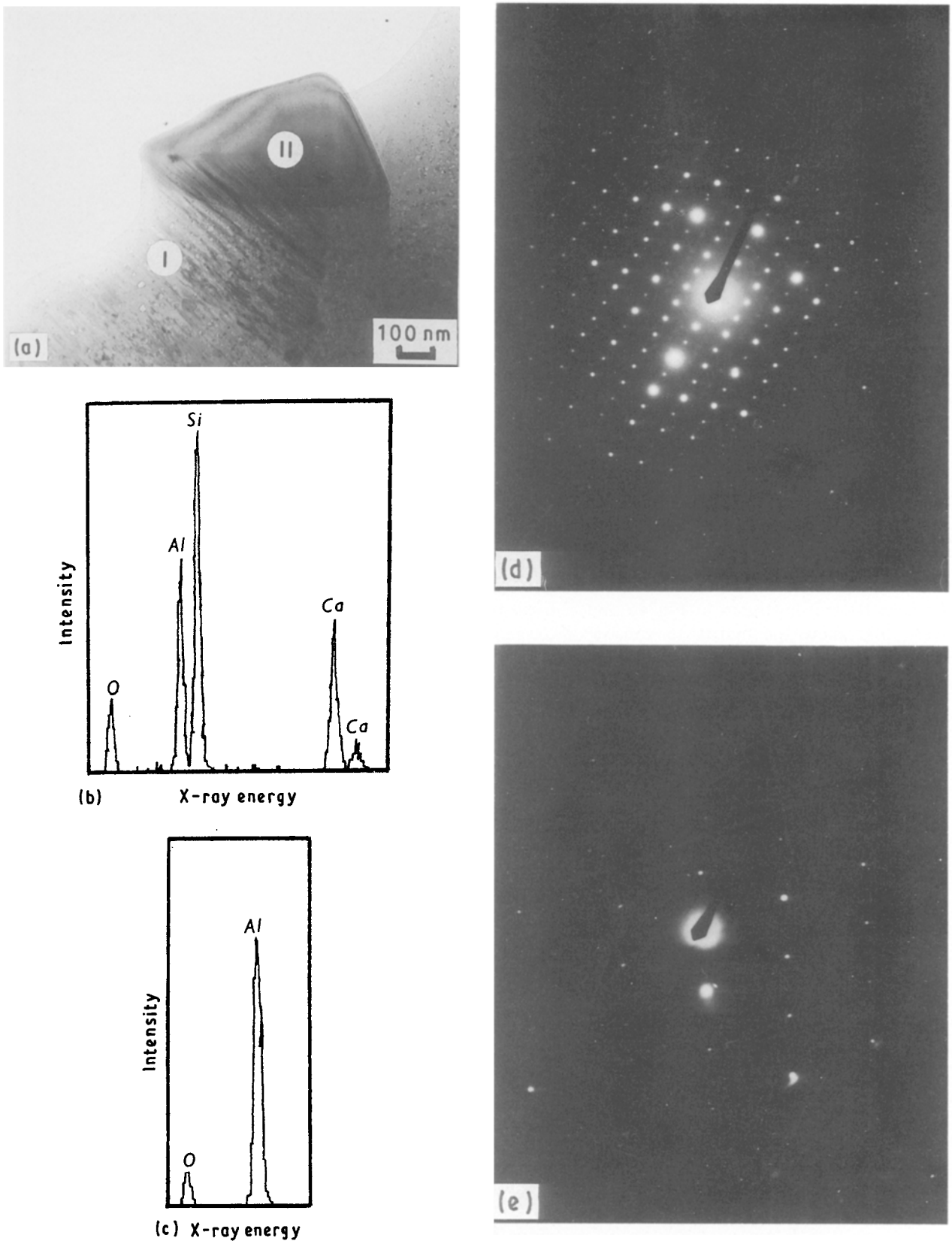

Figure 4 (a) Transmission electron micrograph of a second-phase particle in a CAS matrix. (b) EDS of the CAS matrix. (c) EDS of a second-phase particle. (d) SAD of the CAS matrix. (e) SAD of a second-phase particle.

in accord with that shown in Fig. 5b. The EDS spectrum from the fibre, Fig. 7b, showed the presence of carbon, oxygen and silicon, as expected from the fibre specification. The particle at the interface was rich in zirconium, Fig. 7c, and is probably related to the particles observed at the grain boundaries. The interfacial region (the light band) was enriched in carbon, Fig. 7d, and is probably graphitic.

The mechanical properties of the unidirectional and $(0°/90°)_{3s}$ composites are presented in Table I. The values reported are mostly averages of three or four test results, and no genuine assessment of variability

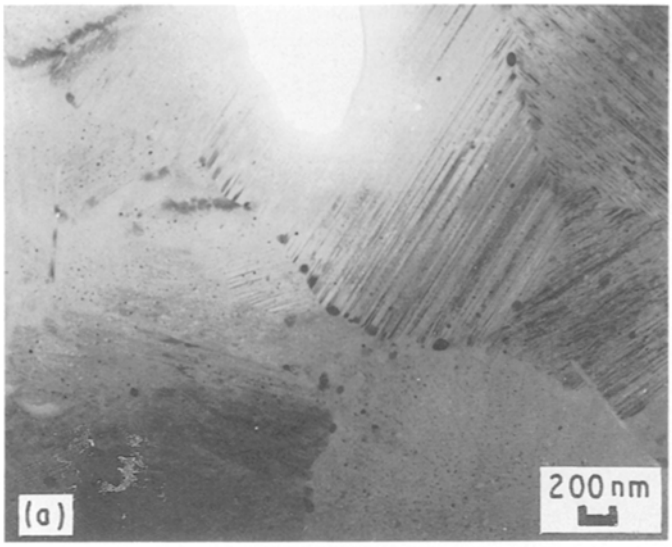

Figure 5 (a) Transmission electron micrograph of the CAS matrix. (b) EDS of a grain-boundary particle.

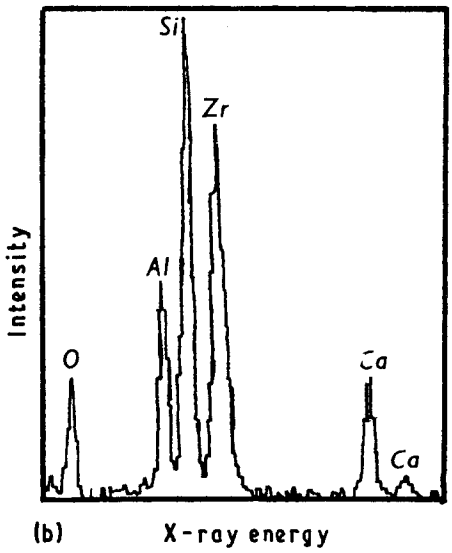

can be given. Fracture surfaces of both unidirectional (Fig. 8) and $(0°/90°)_{3s}$ plates exhibited fibre pull-out with clean fibre surfaces.

3.2. Heat-treated material (CU1 and CX2)

The as-received plate had a smooth surface which still bore pressing marks lying approximately at right angles to the fibre alignment, Fig. 9a. Where fibres lay very close to the surface, chipping of the matrix above the fibres occurred to reveal smooth fibre surfaces. The surfaces of plates heated at 600 and at 800 °C were very similar to that of the as-received condition. After heating at 1000 °C, Fig. 9b, the exposed fibres were rougher in appearance and there was evidence of attack on the matrix. The surface of the plate heated at 1200 °C was very different, Fig. 9c. Where fibres were exposed at the surface, they had been heavily attacked, in some cases degrading totally. The numerous holes in the matrix near fibres suggest that gas evolution has occurred in these regions. Small particles, P, had formed at the surface of the matrix and these were shown by EDS to contain zirconium, oxygen, aluminium, silicon and calcium.

The origin of the holes in the matrix of the 1200 °C treated plate can be deduced from BEI analysis of polished sections. Fig. 10a shows an example where gas has apparently evolved from the fibre/matrix interface. Fig. 10b further indicates that the gas originated from the bulk of the fibre producing voids which have burst through the matrix to leave "blowholes", Fig. 9c. The observed pitting of a fibre surface accords with such a gas evolution process.

The TEM specimens were taken from the surface regions of these heat-treated materials, where the effect of the treatment would be expected to be most evident. The fibre/matrix interface microstructure of as-received CU1 and CX2 plates was very similar to that observed for CX1 (see Fig. 7a), and TEM showed that little change had occurred after heat-treatment at 600 °C.

A transmission electron micrograph of an interface after treatment at 800 °C is illustrated in Fig. 11. The carbon layer is beginning to degrade, and early stages of void formation can be seen at the points marked A. After heat-treatment at 1000 °C, further evidence of degradation at the interface was observed. Fig. 12a shows voids forming at the interface in the areas marked A and the disappearance of the original carbon layer. In Fig. 12b, further reaction has occurred at the interface, to form a featureless zone between fibre and matrix with pores ~ 200 nm in size produced close to the interface. EDS of the light band, I, which contains the pores, Fig. 12c, shows it to consist primarily of silicon and oxygen. All fibre/matrix interfaces studied in the sample treated at 1200 °C closely resembled Fig. 12b, EDS confirming the presence of silicon and oxygen in all interfacial zones.

Measured interfacial friction stress values, τ_i, are plotted as a function of heat-treatment temperature in Fig. 13; treatment times were 24 h in each case. Each experimental point represents the average of 20 measurements taken from the bulk of the specimen. It can be seen that treatment temperatures up to ~ 1200 °C had little effect on interfacial friction stress for fibres in the sample interior. Fig. 13 also gives the results of measurements on five fibres close to the specimen edge in each test. It can be seen that interface friction stress

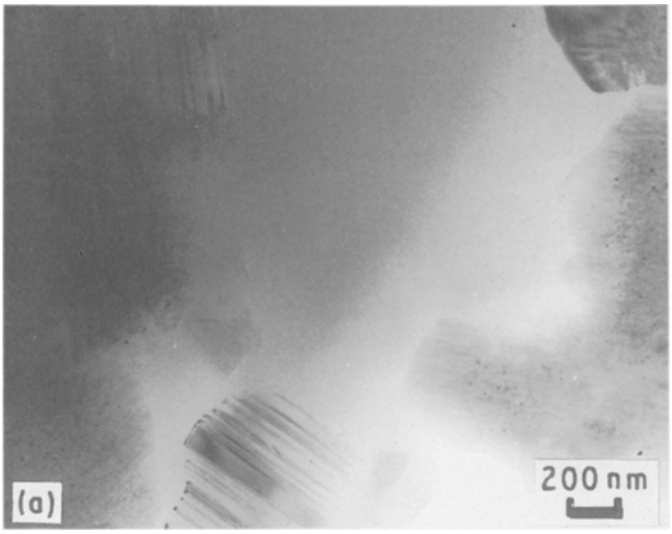

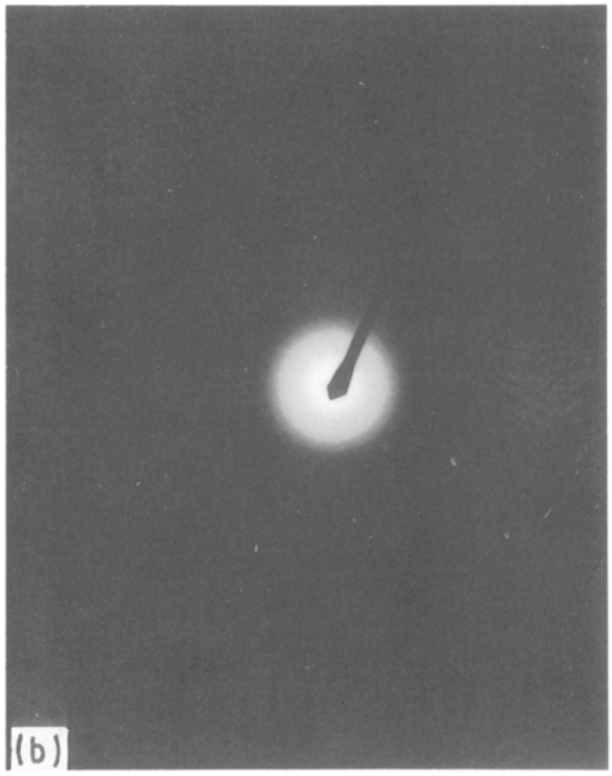

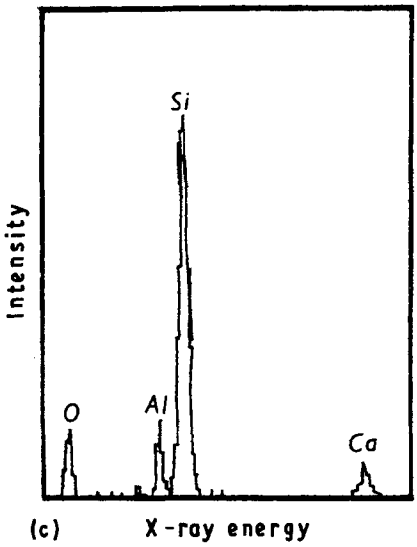

Figure 6 (a) Transmission electron micrograph of the amorphous matrix region. (b) SAD of the amorphous region. (c) EDS of the amorphous region.

TABLE I Composite mechanical properties

Property	$(0)_{12}$	$(0°/90°)_{3s}$
Tensile modulus (GPa)	125	90
Flexural modulus (GPa)	125	115
Poisson ratio	0.25	0.16
Tensile strength (MPa)	330	210
Flexural strength (MPa)	790	530
Interlaminar shear strength (MPa)	40	–

remained fairly constant up to 800 °C and then progressively increased as the heat-treatment temperature was raised to 1200 °C.

The load/deflection curves for the flexural tests were similar in character to that recorded on as-received material, see Fig. 14, irrespective of prior heat treatment. Values of flexural strength are given in Table II and are plotted as a function of heat-treatment temperature in Fig. 15. It should be noted that four measurements were carried out on as-received material and two specimens were tested for each heat-treatment condition. These also show little change with heat-treatment condition, apart from the larger experimental scatter which seemed to characterize the 800 °C heat-treated sample. Examination of fracture surfaces showed very little change in the extent of fibre pull-out in specimens heat treated at 1000 °C and below, all specimens showing pull-out on the tensile surface with crack deflection by the fibres, Fig. 16a. There was, however, a significant change in the fracture behaviour of the outer region of the 1100 °C HT specimen, Fig. 16b. This had broken in a brittle fashion, the fracture propagating across matrix and fibre with essentially no crack deflection at the fibre/matrix interface, Fig. 16c.

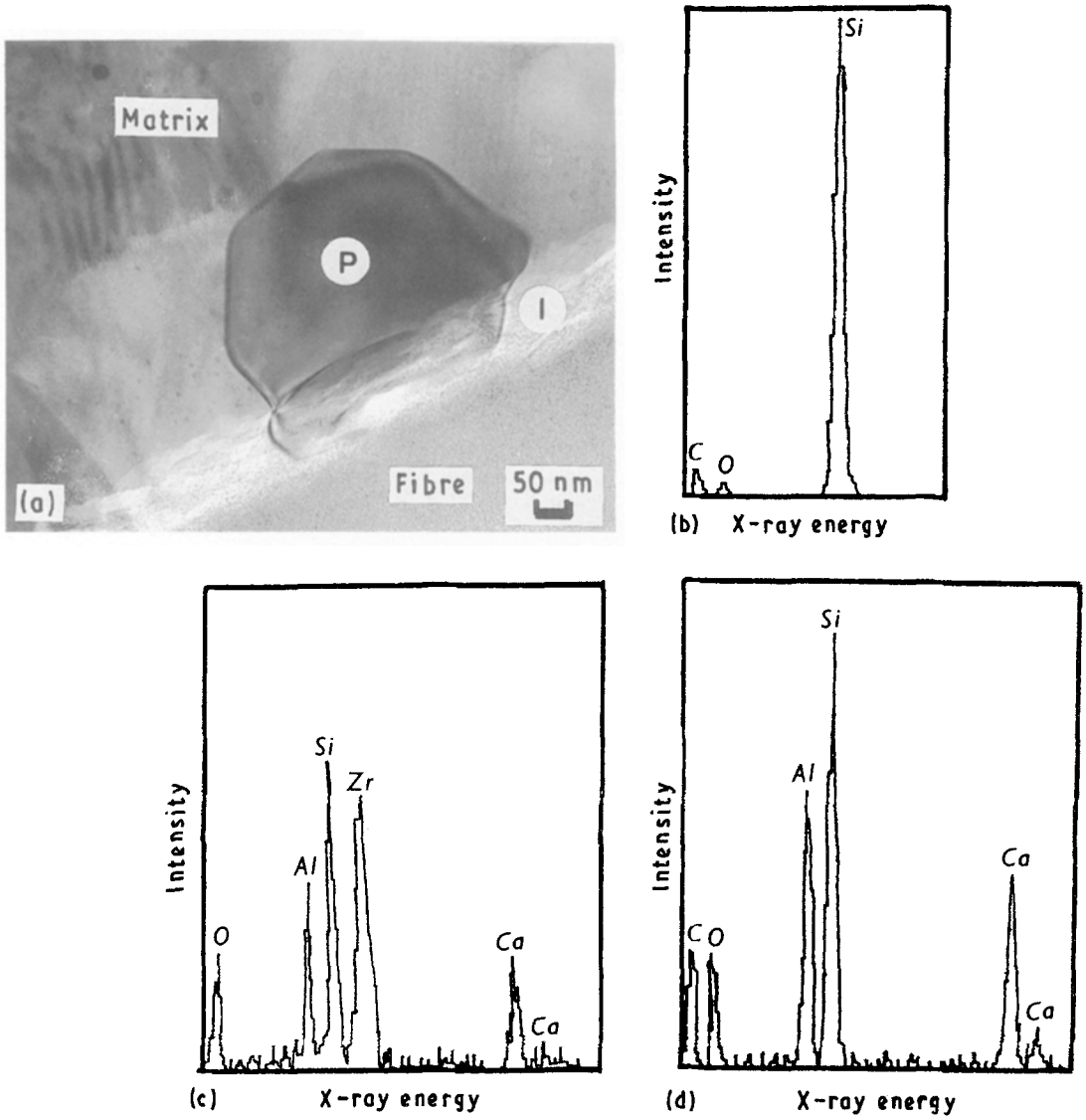

Figure 7 (a) Transmission electron micrograph of the fibre/matrix interface. (b) EDS of the fibre. (c) EDS of the interface particle. (d) EDS of the interface region.

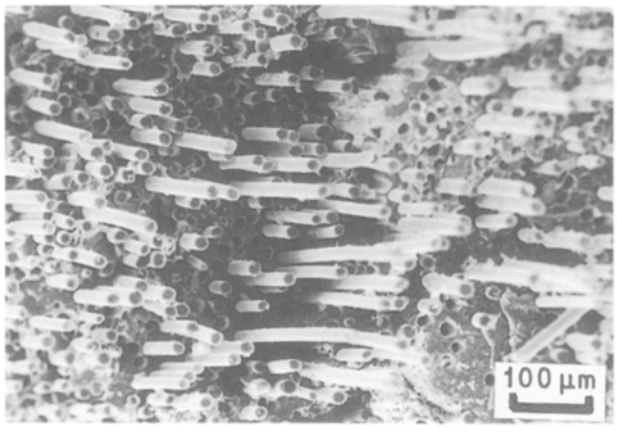

Figure 8 Scanning electron micrograph of the tensile fracture surface of unidirectional Nicalon/CAS.

4. Discussion

The CAS matrix composites were almost fully dense and contained a uniform distribution of fibres amounting to a volume fraction of ~ 0.34.

The matrix of the composites was anorthite, a triclinic crystal structure with the chemical formula $CaAl_2Si_2O_8$ i.e. $CaO \cdot Al_2O_3 \cdot 2SiO_2$. The anorthite phase field in the CaO–SiO_2–Al_2O_3 ternary system is illustrated in Fig. 17. The presence of some second-phase particles, $\sim 2\ \mu m$ in size and identified as alumina, is not surprising because the alumina phase field in the CaO–SiO_2–Al_2O_3 ternary system is very close to the stoichiometric anorthite composition and any local compositional variation in the matrix would encourage transformation to the other phase. The small amount of alumina was, of course, too small to be detected by the XRD technique.

Amorphous glassy regions, comprising less than 0.5 vol % of the matrix, have been detected which were richer in silicon than the surrounding crystalline matrix. No evidence of nucleating agents was found in their vicinity and they are possibly remnants of crystallization.

TEM studies have identified fine (~ 10 nm diameter) zirconium-containing particles within anorthite grains, as well as the slightly larger (~ 50 nm) zirconium-rich particles along grain boundaries. Occasionally, even larger zirconium-rich particles (~ 200 nm) were detected at the fibre/matrix interface.

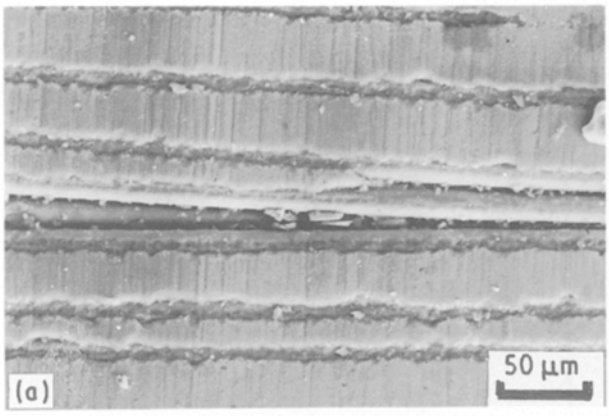

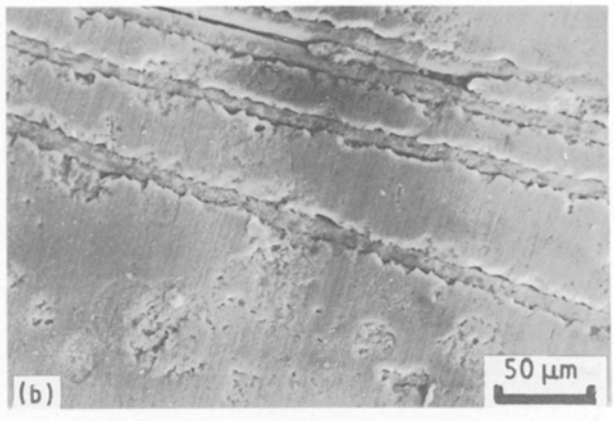

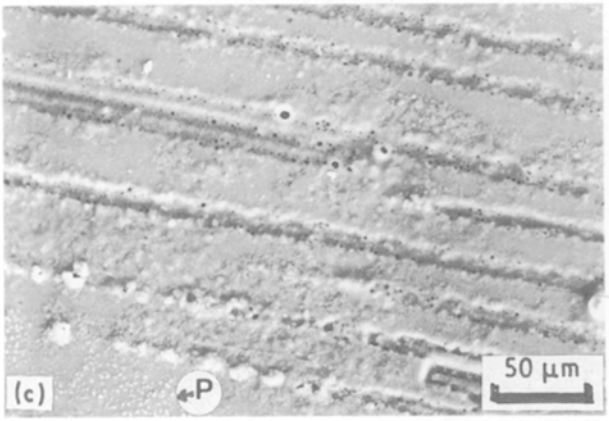

Figure 9 Scanning electron micrographs of surface of (a) as-received Nicalon/CAS, (b) 1000 °C HT Nicalon/CAS, and (c) 1200 °C HT Nicalon/CAS.

The presence of these particles suggests that ZrO_2 may have been used as a nucleating agent in the preparation of the matrix material. Zirconia has been noted to act as an intermediate oxide in the formation of glass networks [11], but its value as a nucleating agent is less well documented. Tashiro [12] reported the use of ZrO_2 in combination with P_2O_5 and noted improved nucleation, but the effect was attributed more to the action of P_2O_5 than ZrO_2. Improved nucleation has also been recorded for a mixture of MoO_3 and ZrO_2 [13], a combination giving also a finer grain size and superior mechanical properties compared with use of a single-oxide nucleating agent. More recently, zirconium compounds have been used in glass-ceramic matrices [14, 15], where the limited solubility of ZrO_2 in the glass melt leads to the presence of crystallites which act as small (~ 5 nm) heterogeneous nucleation sites for crystal growth. The glass viscosity is also reduced by the presence of ZrO_2, and this lowers the activation energy for crystallization. Excess ZrO_2 was seen at grain boundaries in the Li_2O–Al_2O_3–SiO_2 system, similar to the particles observed at grain boundaries in our material.

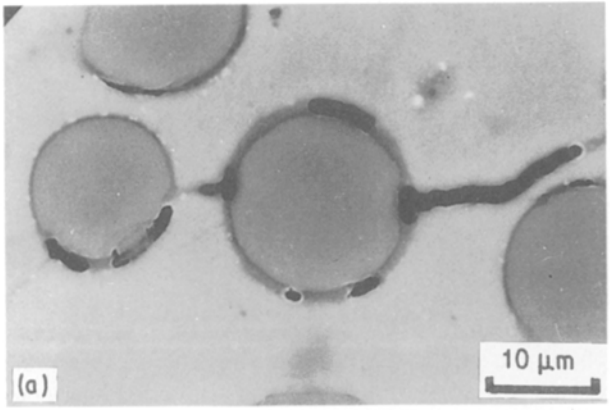

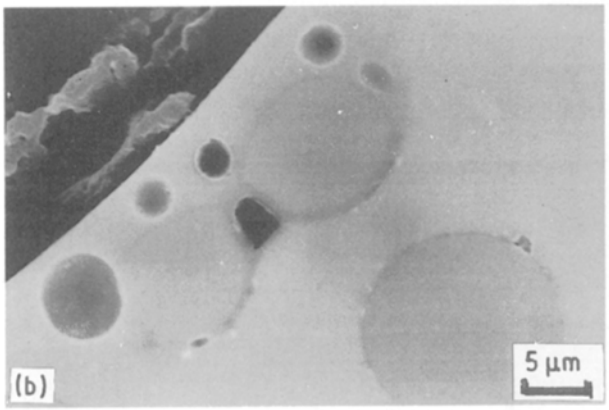

Figure 10 (a) BEI of polished 1200 °C HT Nicalon/CAS, showing degradation of the fibre/matrix interface. (b) As (a), showing degradation of a fibre close to the surface.

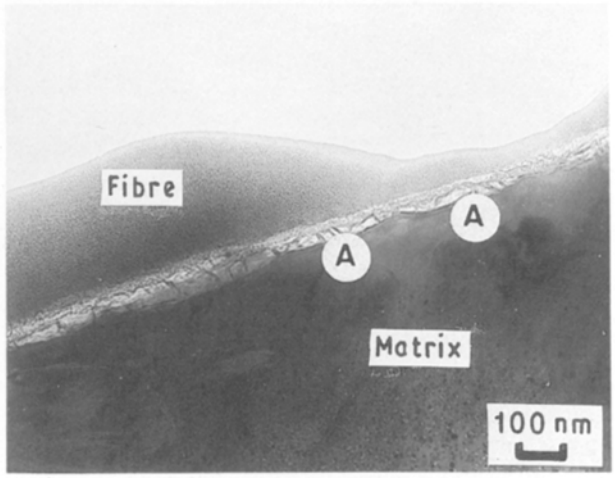

Figure 11 Transmission electron micrograph of fibre/matrix interface in 800 °C HT Nicalon/CAS.

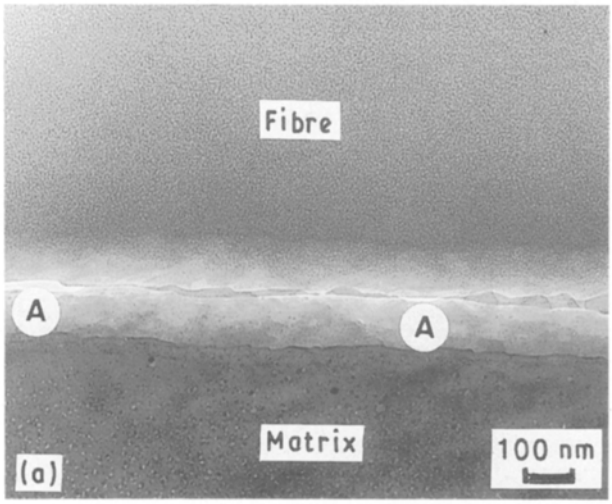

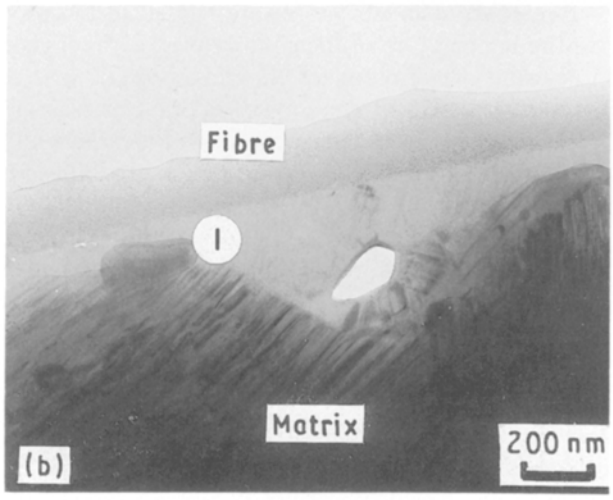

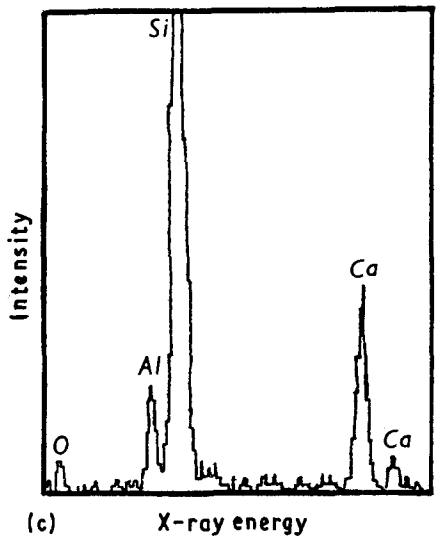

Figure 12 (a) Transmission electron micrograph of fibre/matrix interface in 1000 °C HT Nicalon/CAS. (b) As (a), showing formation of a featureless zone between fibre and matrix. (c) EDS of the featureless zone.

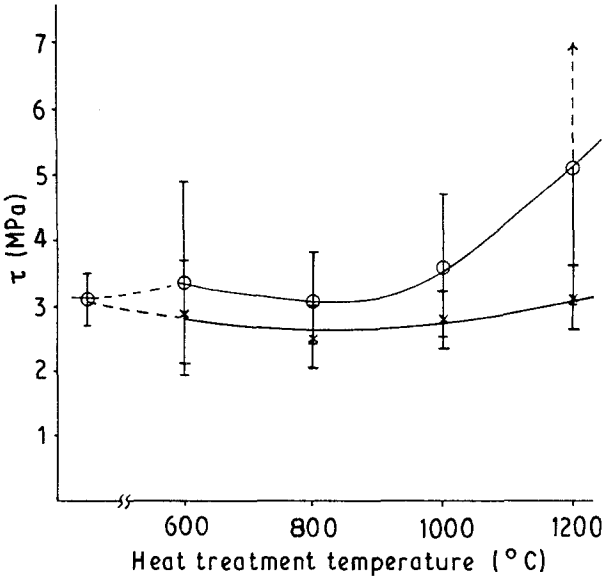

Figure 13 Graph of interfacial friction stress versus heat-treatment temperature for Nicalon/CAS, (×) bulk, (○) edge.

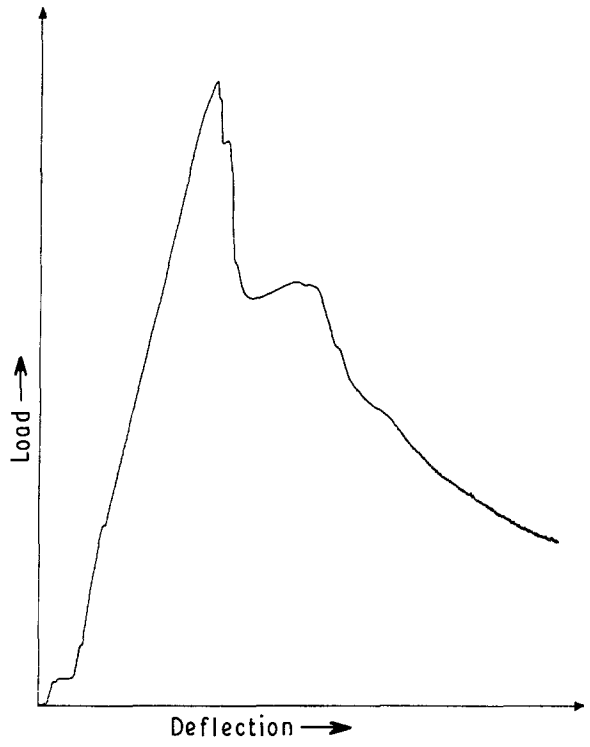

Figure 14 Load versus deflection curve for 600 °C HT Nicalon/CAS in three-point flexure.

The fibre/matrix interfacial region shows evidence of a reaction between fibre and matrix. The reaction zone is visible as a more electron-transparent region ~ 100 nm thick which is enriched in carbon. This indicates that the silicon carbide constituent of the Nicalon fibre and the oxygen in the matrix have reacted according to

$$SiC_{(s)} + O_{2(g)} \rightarrow SiO_{2(s)} + C_{(s)} \quad (3)$$

Such a reaction has been found by Cooper and Chyung [8] in studies on LAS and CAS matrices reinforced with Nicalon, and graphitic interfacial layers have been reported in several other Nicalon-reinforced glass-ceramic composite systems [7, 14]. The graphitic reaction layer formed in the present CAS/Nicalon material contrasts with our earlier findings on the Pyrex/Nicalon system [16], which identified a diffusion band enriched in sodium and trace

TABLE II Values of flexural strength and interfacial friction stress for heat-treated unidirectional Nicalon/CAS.

	Heat-treatment temperature (°C)					
	As-received	600	800	1000	1100	1200
Flexural strength (MPa)	792 840 675 725	647 781	638 867	824 785	856 742	–
Interfacial friction stress interior region (MPa)	3.1 ± 0.4	2.9 ± 0.7	2.5 ± 0.5	2.8 ± 0.5	–	3.1 ± 0.5
Interfacial friction stress surface region (MPa)	–	3.4 ± 1.5	3.1 ± 0.7	3.5 ± 1.1	–	5.1 ± 2.1[a]

[a] Upper limit in excess of 25 MPa.

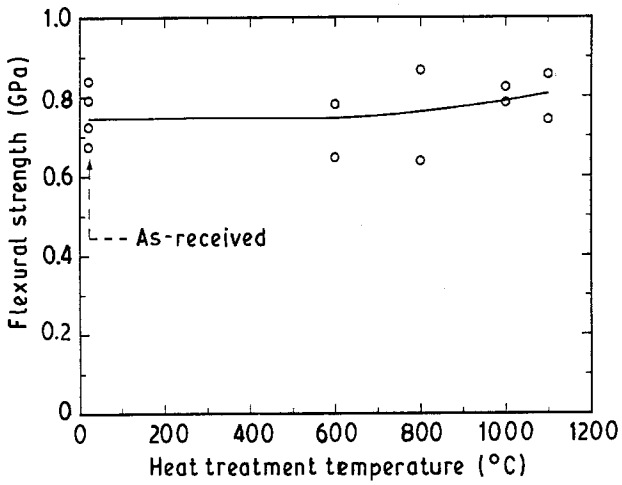

Figure 15 The effect of heat treatment on the flexural strength of unidirectional Nicalon/CAS.

elements such as potassium and calcium in the outer ~ 100 nm fibre but a less extensive carbon reaction layer. It may be argued that the differences in these two interface microstructures are related to the processing temperature of the composites, i.e. the higher processing temperature for the glass-ceramic matrix composite promoted the above reaction, whereas the lower manufacturing temperature for Pyrex/Nicalon, although high enough to encourage sodium diffusion, was insufficient to form substantial amounts of carbon.

When composites were exposed to oxidizing environments at elevated temperature, changes in interface microstructure began to occur after 24 h at 800 °C. There were signs of a volatile-producing reaction, with small voids appearing at the interface, Fig. 11. Void formation was more apparent in samples heated to 1000 and 1200 °C, as was the light featureless zone at the interface which was found to contain silicon and oxygen. The zone results from the formation of silica by oxidation of fibre according to

$$SiC_{(g)} + 2O_{2(g)} \rightarrow SiO_{2(s)} + CO_{2(g)} \text{ or } CO_{(g)} \quad (4)$$

$$C_{(s)} + O_{2(g)} \rightarrow CO_{2(g)} \text{ or } CO_{(g)} \quad (5)$$

The gaseous nature of the products formed in both reactions would thus account for the presence of voids at the interface. Evidence of degradation of both fibre

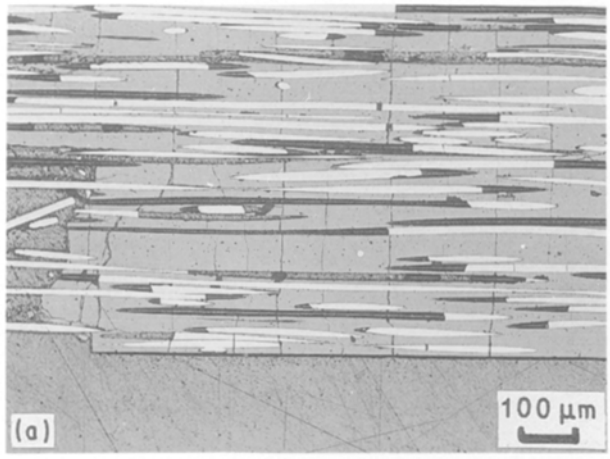

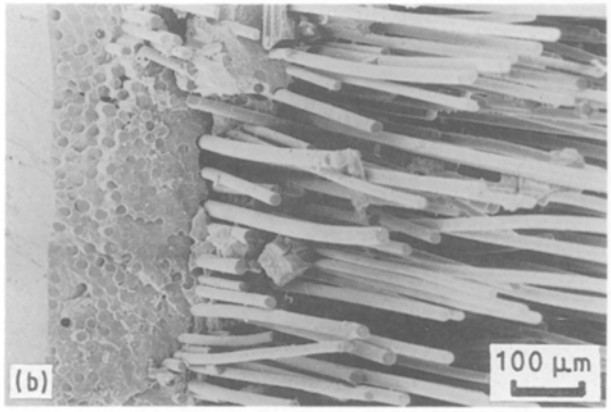

Figure 16 (a) Optical micrograph of the tensile surface of 600 °C HT Nicalon/CAS broken in flexure. (b) Scanning electron micrograph of the tensile surface of 1100 °C HT Nicalon/CAS broken in flexure, showing embrittled zone. (c) Optical micrograph of the tensile surface of 1100 °C HT Nicalon/CAS broken in flexure.

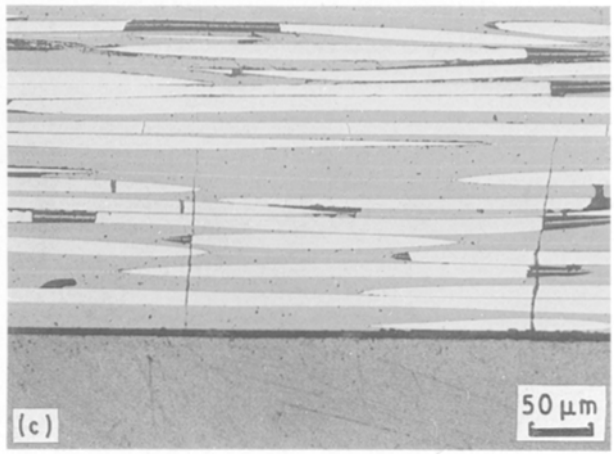

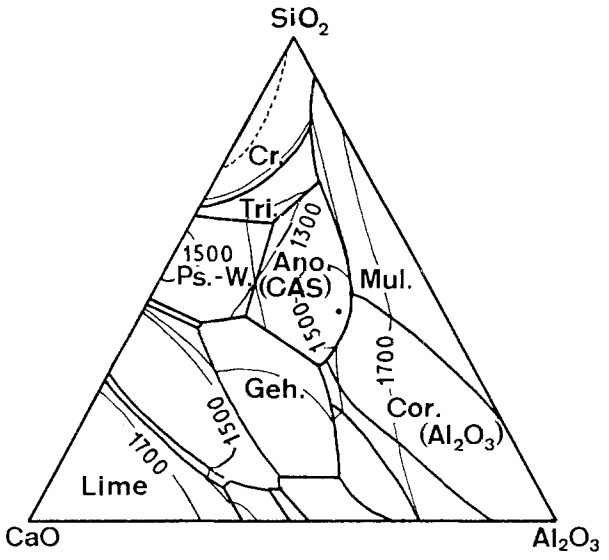

Figure 17 $CaO–Al_2O_3–SiO_2$ ternary phase diagram. Cr = Cristobalite, Tri = tridymite, Ps-W = pseudo Wollastonite, Mul = mullite, Geh = gehenlenite, Cor = corunclum, Lime = CaO, Ano = anorthite.

and interface by these mechanisms is seen in Fig. 10a and b, taken from a sample heated at 1200 °C. The surface of this plate, Fig. 9c, also showed features associated with extensive gas evolution, such as "blowholes" in the matrix which followed the length of subsurface fibres.

The change in the microstructure of the fibre/matrix interface can be correlated with values of interfacial friction stress obtained by the micro-indentation technique. For example, no change in interface microstructure was recorded in interior regions after treatment up to 600 °C and no change in interfacial friction stress values was found. At the surface of the 800 °C sample, oxidation of the carbon interface and of the outer layer of the fibre occurred and a strong bond was established between the matrix and the surface layer of silica on the fibre. This was again reflected in interfacial friction stress values which showed a progressive increase with increase in treatment temperature up to 1200 °C, the highest temperature examined. Voids formed at the interface, but there appeared to be insufficient porosity to weaken the bond significantly.

It may be concluded that the rate of oxidation will be controlled by the diffusion rate of oxygen through the anorthite matrix and/or along grain boundaries and flaws. This process will be faster at higher temperatures, and hence samples heated at higher temperatures show more severe oxidation effects.

The predicted tensile strength of a unidirectional composite from the basic mixture rule is of the order of 610 MPa, assuming mean fibre and matrix strengths of about 1.5 GPa and 150 MPa, respectively, and $V_f = 0.34$. This is nearly twice the experimental value, and rough calculations of the strengths of the other laminates on the basis of the Krenchel orientation factor, $\Sigma a_n \cos^4\theta$ (where a_n is the proportion of fibres at an angle θ to the stress direction), also give predicted values between 1.5 and two times the measured values (Table I). The manufacturer's data sheet gives values of 444 and 194 MPa for the strengths of the unidirectional and $(0°/90°)_{3s}$ composites, respectively. The latter is in agreement with our own result, but whilst the highest value that we obtained from one unidirectional test plate was ~ 400 MPa the former appears much higher than our average value. Prewo [17] reports tensile strengths of 455–680 MPa for cerammed Nicalon/LASII composites, and Kim and Katz [18] obtained a tensile strength of 416 MPa for a Corning-manufactured Nicalon/barium osumilite (BMAS) glass-ceramic matrix composite.

The flexural strengths of all composites are higher, by a factor of between 1.5 and 2.5 depending on lay-up, than the tensile strengths. The value of 793 MPa for the unidirectional composite is somewhat below the range 0.9–1.1 GPa reported by Prewo [17] for Nicalon/LASII composites manufactured by a similar process, but greater than the earlier values of ~ 600 MPa also given by Prewo and Brennan for similar materials [19, 20] and 703 MPa of Kim and Katz [18] for Nicalon/BMAS composite. It is also more in accord with our predicted tensile strength of ~ 650 MPa referred to earlier in relation to an *in situ* fibre strength of ~ 1.5 GPa.

The Aveston, Cooper and Kelly (ACK) theory [21–23] gives the limiting crack separation in a brittle matrix composite as being between x' and $2x'$, where

$$x' = (V_m/V_f)\,\sigma_{mu}\,r/2\tau_i \qquad (6)$$

σ_{mu} being the failure stress of the unreinforced matrix, r the fibre radius, and τ_i the interfacial shear stress. Aveston *et al.* [23] show that the mean crack spacing is given by $1.364x'$. In our room-temperature deformation experiments, we obtained average crack spacing values of the order of 0.2 mm, which implies a value of x' of 0.15 mm. This indicates that the interfacial shear stress, τ_i, must be between about 4 and 6 MPa, depending upon whether a value of 100 or 150 MPa is taken for σ_{mu}. Evans [24] cites a τ_i value of 9 MPa for a Nicalon/CAS composite, compared with only 2 MPa for a Nicalon/LAS composite from similar calculations, which is slightly higher than found in these studies, although it is not known what value of σ_{mu} is taken for CAS. We note that the values of τ_i of 3–5 MPa obtained by the microindentation method agree well with the 5 MPa derived from ACK theory, given the assumptions made in deriving the two results. After heat treatment at 600 °C the average crack spacing is about 0.1 mm, but with a wide spread of individual values. The derived value of τ_i is therefore apparently about twice that for as-received materials, say about 10 MPa. As we have seen from Fig. 13, however, the mean value of τ_i derived from the microindentation experiments is unaffected by heat treatments up to 600 °C, only the variability increasing as a result of the exposure. Given the fact that the variation in the crack spacings is of the order of $\pm$ 50%, it is not possible to reconcile the values of τ_i obtained in these two different ways after heat treatment.

Although it is evident that oxidation effects had produced a change in microstructure of the fibre/matrix interfaces in the surface zone, leading to an embrittled region, this was not reflected in a significant

drop in flexural strength. Thus it would appear that Nicalon/CAS composites can survive short-term exposure to oxidizing atmospheres in an unstressed condition without severe detriment to mechanical performance. This is not, however, expected to be the case if the material is stressed at high temperature, because the formation of matrix microcracks will provide a fast transport route for oxidants to the composite interior and lead to faster embrittlement than if matrix diffusion alone controlled the oxidation rate.

Acknowledgements

The authors acknowledge the financial support of Rolls Royce plc and RAE Pyestock, the SERC for funding of the Electron Optics facilities, and the Reverend B. Chapman for XRD studies.

References

1. R. A. J. SAMBELL, A. BRIGGS, D. C. PHILLIPS and D. H. BOWEN, *J. Mater. Sci.* **7** (1972) 676.
2. D. C. PHILLIPS, *ibid.* **9** (1974) 1847.
3. S. YAJIMA, K. OKAMURA, J. HAYASHI and M. OMORI, *J. Amer. Ceram. Soc.* **59** (1976) 324.
4. K. M. PREWO and J. J. BRENNAN, *J. Mater. Sci.* **17** (1982) 1201.
5. A. BRIGGS and R. W. DAVIDGE, *Mater. Sci. Engng* **A109** (1989) 363.
6. J. J. BRENNAN and K. M. PREWO, *J. Mater. Sci.* **17** (1982) 2371.
7. E. BISCHOFF, M. RÜHLE, O. SBAIZERO and A. G. EVANS, *J. Amer. Ceram. Soc.* **72** (1989) 741.
8. R. F. COOPER and K. CHYUNG, *J. Mater. Sci.* **22** (1987) 3148.
9. D. B. MARSHALL and A. G. EVANS, *J. Amer Ceram. Soc.* **68** (1985) 225.
10. I. Y. BORG and D. H. SMITH, *Amer. Mineral* **53** (1968) 1709.
11. P. W. McMILLAN "Glass-Ceramics" (2nd Edn Academic Press, London, 1979) p. 14.
12. M. TASHIRO, *Glass Ind.* **47** (1966) 428.
13. P. W. McMILLAN and D. C. LAWTON Brit. Pat. no. 1067392. (1967)
14. R. CHAIM and A. H. HEUER, *Adv. Ceram. Mater.* **2** (1987) 154.
15. J.-Y. HSU and R. F. SPEYER, *J. Amer. Ceram. Soc.* **73** (1990) 3585.
16. S. M. BLEAY and V. D. SCOTT, *J. Mater. Sci.* **26** (1991) 2229.
17. K. M. PREWO, *J. Mater. Sci.* **21** (1986) 3590.
18. R. Y. KIM and A. P. KATZ, *Ceram. Engng Sci. Proc. (Amer. Ceram. Soc.)* **9** (1988) 853.
19. K. M. PREWO and J. J. BRENNAN, *J. Mater. Sci.* **15** (1980) 463
20. *Idem., ibid.* **17** (1982) 1201.
21. J. AVESTON, G. A. COOPER and A. KELLY, "The Properties of Fibre Composites" (IPC Science and Technology Press, Guildford, 1971) pp. 15–26
22. J. AVESTON and A. KELLY, *J. Mater. Sci.* **8** (1973) 352.
23. J. AVESTON, R. A. MERCER and J. M. SILLWOOD, "Composites-Standards, Testing and Design" (IPC Science and Technology Press, Guildford, 1974) pp. 93–102.
24. A. G. EVANS, "Mechanical and Physical Behaviour of Metallic and Ceramic Composites", edited by S. I. Andersen, H. Lilholt and O. B. Pedersen (Risø, Denmark, 1988) pp. 13–34.

Received 16 September
and accepted 26 September 1991